A numerical study of charge transport properties and an influence of buffer nano-layers on J-V characteristics of organic solar cells
(Thesis abstract)

Candidate: Tran Van Hung (email: hungtran.vnu@gmail.com)
Supervisor: Dr. Dang Dinh Long (email: longdd@gmail.com/v.longdd6@vinschool.com)

I. Introduction

Over the past few decades, organic solar cells (OSCs) based on the use of donor:acceptor blends as carrier generator as well as transport have attracted tremendous attention because of their potentials such as low-cost, flexible, lightweight, portable and large-area energy-harvesting devices. Two main approaches can possibly be applied in order to improve the overall power conversion efficiency (PCE) including either modification of the constinuents of photoactive layer or introduction of charge carrier transport/blocking (buffer) layers. It has empirically been proved that a considerable enhencement of PCE is observed thanks to the insertion an interfacial layer between active layer and electrode [1]. Beside of that, works have also been done with modifying the active layer and gave trivial increase of PCE. In this work, we use theoritical simulation aiming at proving the effectiveness of both cases. Regarding buffer layer, we applied single diode model in multilayer organic solar cells and simulated its working principle as well as proposed a method to extract parameters of interest from experimental J-V curves with high accuracy. We also investigated the conversion from the power factor to efficiency effected by buffer layer thickness in each type of organic solar cell. The influence of thickness to device properties is figured out to be very clear and in good accordance with experimental data. Finally, the work also focus typically on analyzing charge transport of organic materials by Monte Carlo method [2]. By this way, we can also investigate the influence of parameters such as temperature, electric field on electrical properties of materials.

I.1 Organic solar cells

In general, organic solar cells have a multilayer structure including active layer, electrodes, and interfacial layers [3]. The photoactive layer consists of two constituents including a donor material which is usually a conjugated polymer or oligomers in conjunction with an acceptor material which is often fullerene derivative. The photoactive layer is inserted between anode and cathode electrodes in which at least one electrode is transparent. In addition, in order to enhance the performance of solar cells, the interfacial layers called hole conducting layer and electron conducting layer are located between anode-photoactive and cathode-photoactive interfaces, respectively. Recently inverted architecture has been applied for organic solar cells where the cathode is considered as transparent electrode while the opaque other is anode. The fact that efficiency of inverted devices is comparable with the conventional devices but the stability is much better in environment [4]. Schematics of both conventional and inverted solar cells are illustrated in Fig. 1a.

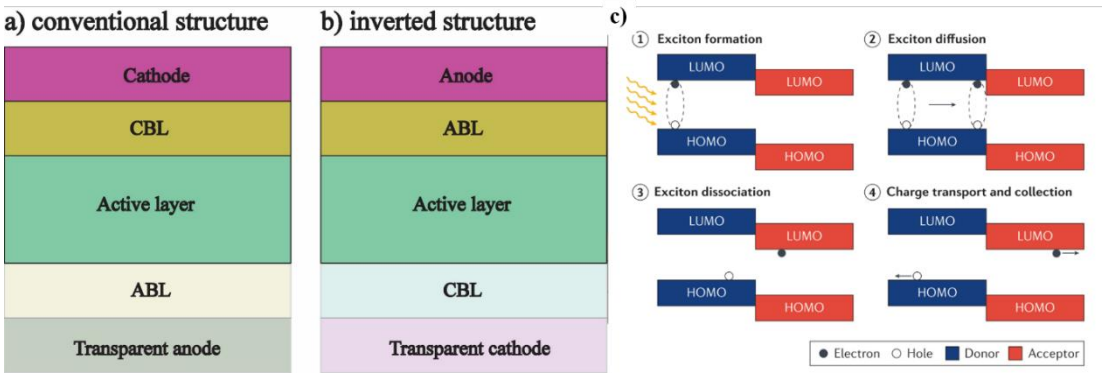

Figure 1: Two fundamental organic solar cell structures (a,b) and (c) working mechanism of organic solar cells (reprinted) [5]. Where CBL denotes cathode buffer layer, ABL denotes anode buffer layer, LUMO denotes lowest unoccupied molecular orbital, and HOMO denotes highest occupied molecular orbital.

The working mechanism can be seen in four fundamental steps as shown in Fig. 1c; (1) when light is absorbed by donor material, electrons are excited from highest occupied molecular orbital (HOMO) to lowest unoccupied molecular orbital (LUMO). As a result, the electron-hole pairs with biding energies in a range of 0.1 eV and 0.4 eV are generated because of low mobility of organic materials. (2) the excitons diffuse to the donor-acceptor interface, (3) where they are separated into free carriers (electrons and holes) due to the offset potential energy at donor-acceptor interface. (4) Charge carriers diffuse to respective electrodes through continuous pathway and avoid recombination or traps [6].

I.2 The role of buffer layers

Due to the poor photoactive-electrode interfaces, interfacial layers must be established to adjust the band alignment at the interface, select one type of carriers, prevent chemical reaction between electrodes and photoactive layer, improve stability in environment, and act as optical spacer [7-10]. There exist two types of buffer layers commonly used in organic solar cells including anode and cathode buffer layers. They correspond to the layers inserted at anode/photoactive layer (hole blocking layer) and cathode/photoactive layer interface (electron blocking layer). More importantly, buffer layers can play an important role in improvement of photocurrent [11]. For the anode buffer layers, they play a role of improving the anode electrode efficiency including the collection and extraction of positive carriers. To really have that improvement, an anode buffer layer needs to satisfy some requirements: (1) forming an ohmic contact with the donor material; (2) allowing positive carriers transport and blocking negative carriers, (3) the series resistance of device should low as possible when ABL insert in device, and (4) having transparent property in the conventional configuration. An anode buffer layer can be either inorganic such as V_2O_5, MoO_3, WO_3, NiO and Cu_2O or organic such as poly(3,4-ethylenedioxithiophene):poly(styrene sulfonic acid) PEDOT:PSS. For the cathode buffer layers, they take a role as improving the cathode electrode efficiency in the collection and extraction negative charge carriers. They also fulfill with following requirements: (1) forming an ohmic contact with the acceptor material, (2) allowing negative carrier transport as well as blocking positive carriers, (3) the series resistance of device should low as possible when ABL insert in device, and (4) having transparent property in the inverted configuration [7]. Similarly, a cathode buffer layer can be either inorganic such as LiF, TiO_x, CaO and ZnO or organic such as pyronin B, pentadecafluororooctyl phenyl-C_{60}-butyrate F-PCBM, and so on.

II. Simulation methods

For semiconductors and solar cells, ones likely to employ simulation methods equivalent to different levels of difficulty such as quantum mechanism, Monte Carlo technique, classical analysis, and equivalent circuit. In this work, I going to apply two simulation models including equivalent circuit and Monte Carlo simulation. We first start with single diode model to interpret the the working principle of organic solar cell. This model reflects the non-liner relationship between $J-V$ characteristic and five electrical parameters series resistance, shunt resistance, photocurrent, saturation current and diode ideality factor. On the other hand, the charge transport mechanism in organic semiconductor was studied by Bässler model with assistance of Monte Carlo technique [12]. In the later model, the semiconductor film is assumed as a lattice so that simulation of charge transport mechanism through the film could be performed. In fact, this model particularly reveals the charge carrier transport property in micro scale.

II.1 Single diode model

In general, the simple approach to evaluate performance of an organic solar cell is based on analyzing $J-V$ under given temperature and irradiation condition. From an experimental curve, it can show some solar cell parameters such as short circuit current density, open circuit voltage, fill factor, and power conversion efficiency. However, to evaluate the other electrical parameters including series resistance and shunt resistance, we need to rely on a physical model. Analytical model as diode model is used to study and evaluate behavior of organic solar cell because of its balance between accuracy and difficulty. To understand the construction of single diode model we should notice that a solar cell consists of two main different layers of semiconductor materials putting together and other buffer layers [13, 14].

In the dark region, a single-junction solar cell behaves similarly to a semiconductor diode and $J-V$ characteristic is described by following Shockley equation.

$$J_s = J_0\left(e^{\frac{qV}{nkT}} - 1\right) \qquad 2.1$$

Where: J_s is dark current, J_0 is the reverse saturation current density, V is applied voltage, q is the electron charge (1.602×10^{-19} C), k is the Boltzmann constant, T is the absolute temperature and n is diode factor depend on the quality of semiconductor.

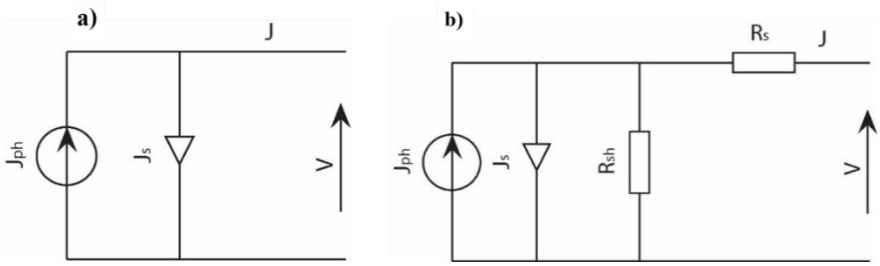

Figure 2: (a) ideal diode model; (b) the single diode for solar cell.

Under the illumination, the cell generates electron-hole pairs that yield a current density J_{ph} - photocurrent density. The solar cell can be represented by a basic electric circuit, which consists of a current source with intensity J_{ph} , and a diode as in Fig 2a. The solar cell has the same behavior as a diode. The J-V characteristic is described by:

$$J = J_{ph} - J_s \qquad 2.2$$

$$J = J_{ph} - J_0\left(e^{\frac{qV}{nkT}} - 1\right) \qquad 2.3$$

In particular, solar cells behave actually in a complex way, especially organic solar cell, therefore, in which leak current cannot be overlooked. The most efficient model to describe the working principle of solar cell is the single diode model as shown in Fig. 2b, and the relation between current and voltage is mathematically defined by the flowing equation:

$$J = J_{ph} - J_0\left(e^{\frac{qV}{nkT}} - 1\right) - \frac{V + JR_s}{R_{sh}} \qquad 2.4$$

Where J and V represent the current density and voltage of solar cell, respectively. J_{ph} is the photo-generated current, J_0 is the reverse bias saturation current density, R_s and R_{sh} represent the series and shunt resistances respectively, n is the diode ideality factor of cell, and V_{th} is thermal voltage of the cell is expressed by $V_{th} = k_B T/q$. Here, k_B is the Boltzmann's constant ($1.3806 \times 10^{-23}\ J/K$), T is the absolute temperature (K), and q is the electron charge ($1.6022 \times 10^{-19}\ C$).

By using the single diode model, this work successfully described the working principle of the multilayers organic solar cell, and examined the relation between buffer layer thickness and power conversion efficiency through analyzing series and shunt resistances from $J - V$ characteristics under given irradiation condition.

II.2 The hopping transport model

It is clear that the analytical model as single diode model only reflects ambient temperature, incident radiation, and the influence on the efficiency of the solar cell. Herein the Monte Carlo technique-based model is given to study charge transport through organic materials as well as organic semiconductors.

The Monte Carlo is a technique for analyzing phenomena by means of computer algorithms based on the generation of random numbers. Monte Carlo method is named from the gambling city in Monaco because of using stochastic process to accept or reject events during solving. Monte Carlo simulation is applied for a wide range of applications of different fields such as science, commerce, and finance. In physics, Monte Carlo technique is suitable to examine systems which have large degree of freedoms including gases, fluids, disordered materials, optical systems, many body particles, quantum physics [15]. Remarkably, the accuracy of the model is higher when system is larger and more complex.

a) Modeling organic molecule and polymer layers

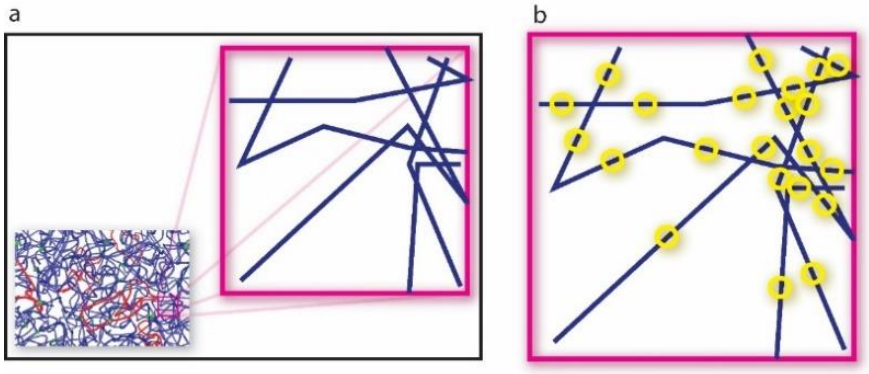

Figure 3: a) Polymer chains. b) Long chains would break into small conjugation units (sites are represented by yellow circles)

To examine charge transport in organic materials the readers should identify how organic layer should be treated? It is well known that a solid polymer film contains a series of polymer chains which distribute over space. It is assumed that the polymer chains are perfectly continuous without kinks and twists, charge carriers are not localized over the whole chains. In practical, the polymer chains in electric device are broken into smaller units by chemical or physical defects. As a result, there are many small electronic units that can consider as either small molecules or segments of the main polymer chain that are separated by topological defects forming the film. In this case, the charge carriers are localized at small units which are called sites. Fig 3b shows an illustration of how polymer chains would be broken into smaller units. Therefore, to simplify the model we only consider the appearance of distribution of electrical sites that can host charge and enable them to move through the film. In summary, what we need now to examine charge transport across the site matrix in real space as well as in energy space shown Fig.4.

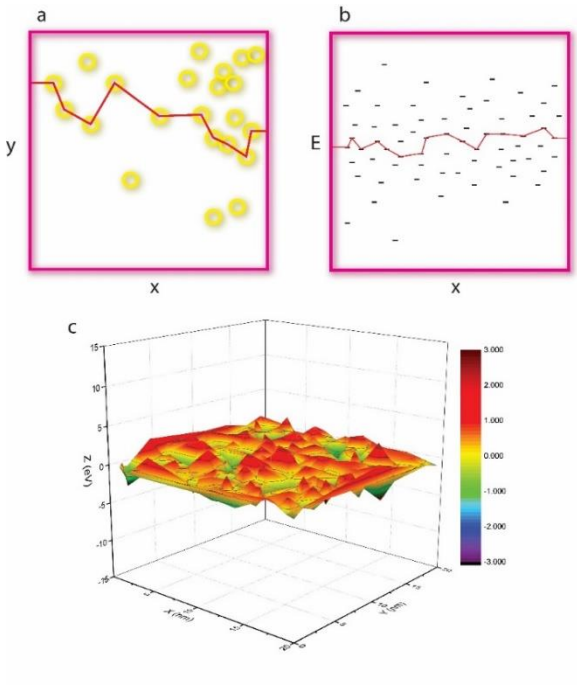

Figure 4: Distribution of sites in real space (a), energy space (b), energy landscape in space (c). Red line is the path electron must take while hopping from one side to the other (under applied electric field).

b) The hopping transition

As we discussed above, the property of charge transport is studied through a distribution of sites of slightly different energies with each other owing to differences in their environments as well as the lengths of segments. In the present model, a carrier is able to tunnel to another that is its vicinity at the same time as it emits or absorbs a phonon. The tunneling process are named as “hops” in hopping transport across localized states. The hopping events from site i to site j are controlled by Miller-Abrahams hopping rate with a spatial separation r_{ij}.

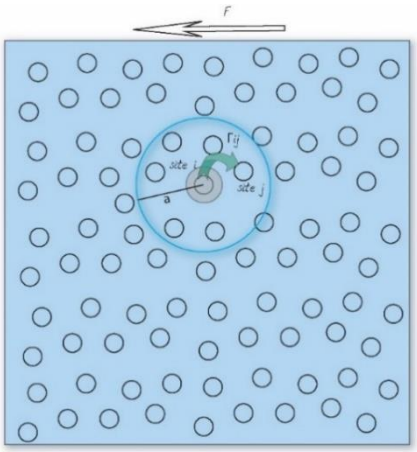

Figure 5: The hop from site to the other site. Where a is cut-off radius and Γ_{ij} is hopping rate.

$$\Gamma_{ij} = v_0 \exp\left(-\frac{2r_{ij}}{a}\right) \begin{cases} \exp\left(-\frac{(\Delta E_{ij})}{k_B T}\right), & E_j - E_i > 0 \\ 1, & E_j - E_i \leq 0 \end{cases} \qquad 2.5$$

Where v_0 is the attempt-to-escape frequency which depends on the phonon frequencies, a is the localization length which describes spatial size of electron wave functions of the localized states, and $\Delta E_{ij} = E_j - E_i$ is the energy difference of two sites. The energy difference would be $\Delta E_{ij} = E_j - E_i - Fe(x_j - x_i)$ under applied electric field F parallel to x direction. It is obvious that the hopping rate between site i and site j depends exponentially on both the distance and the energy difference as well. The exponential function $\exp\left(-\frac{(\Delta E_{ij})}{k_B T}\right)$ multiplied by pre-factor for a transition from a localized state i to a higher energy state j describes the probability of absorbing a phonon. Whereas, for the reverse transition to a lower energy state, a process emits excess energy hold a probability of 1 multiplied by pre-factor as shown in equation 2.5.

By using the Miller-Abraham rate, it is assumed that the sites have no structure, characterized only by their positions and energies. The hopping rate therefore depends on the distance between sites and their energy differences. The modeled polymer in Fig. 5. seems to be very rough approximation, because the hopping rate between two sites also depend on their orientations. To simplify, we omitted the orientation factor. Even omitting that feature, many works were successful to acquire the conducting features of polymers with using the simple model of Miller-Abrahams hopping rate. The last but not least, we also assumed that the charge carriers are only electrons since holes behave same way except for the sign of charge.

c) Distribution of sites in space and energy

In order to calculate the mobility, the positions and energies of all sites are principle inputs that must be known for calculation. The energy distribution of the sites is identified by the density of state (DOS) $g(\varepsilon)$ and relies on the material. The final results are particularly influenced by how we determine distribution because the hopping rate depends not only on the distance between sites but also on the energy difference between them. There are two common energy distributions including exponential distribution for inorganic materials and Gaussian distribution for organic materials. These distributions were established by measuring the optical absorption spectrum and the absorption bands of materials [2]. Hence, for organic materials, the Gauss distribution is selected.

Exponential distribution:

$$g(\varepsilon) = \frac{N}{\varepsilon_0} e^{\left(\frac{\varepsilon}{\varepsilon_0}\right)} \qquad 2.6$$

Here N is the spatial density of sites, ε_0 is the energy scale of the distribution.

Gaussian distribution:

$$g(\varepsilon) = \frac{N}{\sigma\sqrt{2\pi}} e^{\left(-\frac{\varepsilon^2}{2\sigma^2}\right)} \qquad 2.7$$

Where, σ is the standard deviation of the distribution. The energy ε is measured relatively to the center of density of state.

On the one hand, the site distribution is randomly placed in space complying with a uniform distribution. On the other hand, another more effective approach is that the sites are placed on a square lattice in two dimensions or a cubic lattice in three dimensions for computation. Here we chose the latter.

d) Monte Carlo simulation

The simplest approach is that we simulate one single electron moving in the lattice system at a time. In this case the electron density is low, therefore, the interaction between electrons is overlooked. Under applied electrical field electron performs a stochastic motion in the lattice system, and then we collect that stochastic motion. As we mentioned above, the destination site is chosen randomly, but it depends on the hopping rates to each other possible destination site. The time that charge carriers abide each site is also generated randomly and depends on the total hopping rate. After a set of jumps, a statistic of charge carrier trajectory is collected and the transport properties of the material can be determined.

More specific, how a carrier performs a hopping process to a site destination in a group of sites will be described below:

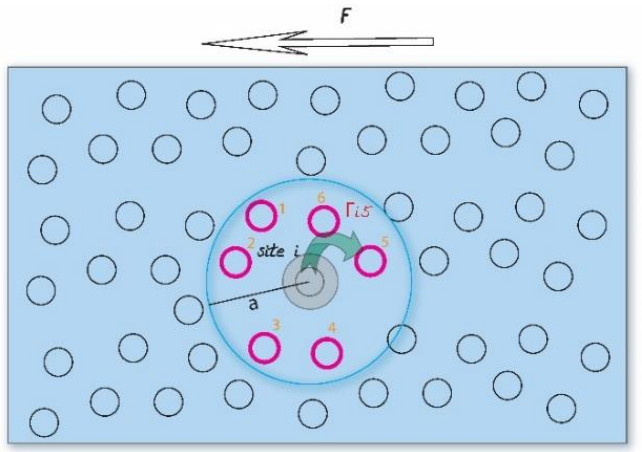

Figure 6: Illustration of site choosing mechanism of an electron.

Where, the pink circles denote the possible sites of destination and the electron are on grey circular shade. In the very short period of time, the electron will hop to one of the possible destination sites, so which one will be chosen. When the charge carrier is located on site i, the value of the total hopping rate (Γ_i) is given by:

$$\Gamma_i = \sum_j \Gamma_{ij} \qquad 2.8$$

In the case of Fig. 6. $\Gamma_i = \Gamma_{i1} + \Gamma_{i2} + \Gamma_{i3} + \Gamma_{i4} + \Gamma_{i5} + \Gamma_{i6}$ with Γ_{ij} is the hopping rate is calculated by Miller-Abraham formula. The probability that a carrier jumps from a site i to any site j is given by:

$$p_{ij} = \frac{\Gamma_{ij}}{\Gamma_i} \qquad 2.9$$

And $\sum_j p_{ij} = 1$

The time τ for a carrier spending on the site i before hopping is calculated as

$$\tau = {}^{T}/_{\Gamma_i} \qquad 2.10$$

Where T is taken from another exponential distribution of random numbers with unit expectation value and unit

variance.

The destination site that the carrier jumps to is determined by picking a random number x between 0 and 1 from a uniform distribution and satisfy the following condition:

$$\sum_{k=1}^{j-1} p_{ik} \leq x < \sum_{k=1}^{j} p_{ik} \qquad 2.11$$

III. Results and discussions

III.1 The influence of buffer layer on performance of organic solar cells

In this section the results of the influence of buffer layer thickness on $J-V$ characteristics as well as performance of organic solar cells: power conversion efficiency (PCE), fill factor (FF), series (R_s) and shunt resistances (R_{sh}) would be given. In order to examine the influence from experiment curves, the simulation technique and the numerical method are applied. Although FF, PCE, can read from experimental data without calculation, however, R_s and R_{sh} are not easily to extract. Here the Ortiz-Conde method based on Lambert function is used to compute all parameters of organic solar cells [16].

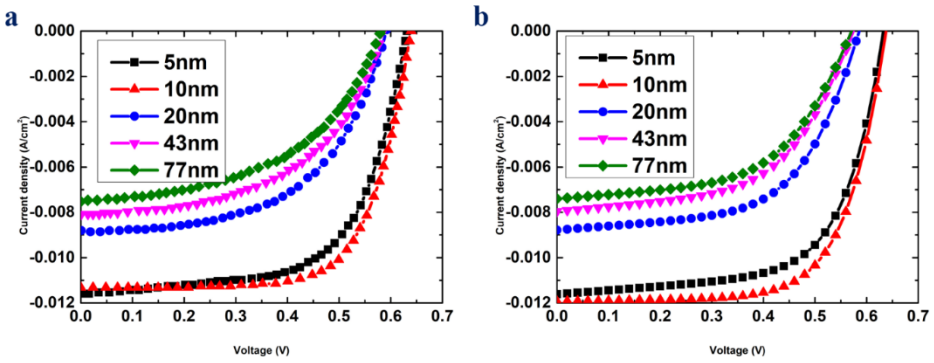

Figure 7: J-V characteristics vary in thickness of NiO with experimental data (a) and simulated data (b)

In order to examine the influence of buffer layer on parameters, we use Irwin's data about organic solar cell with structure of glass/ITO/NiO/PEDOT:PSS/-P3HT:PCBM/LiF/Al in which NiO plays anode buffer layer [17]. From experimental curves we calculated the parameters of solar cell by using numerical method as shown table 1. Fig. 7b. shown that simulated results behave similarly with experimental curves.

The calculated values from experimental data are quite accurate with measurable values, especially FF and PCE (Fig. 8). Clearly, when comparing extracted values and experimental values, the maximum of FF and PCE reach at 10 nm thickness of NiO. For the fill factor, the extracted value and experimental value are 0.678 and 0.693 respectively. For the power conversion efficiency, extracted value and experimental value are 4.9 and 5.16 respectively. Moreover, this extracted method also carries out electrical parameters including series resistance (R_s) and shunt resistance (R_{sh}). At the thickness of maximum power conversion efficiency, the values of R_s and R_{sh} are 1.4 Ω and 3960.108 Ω, respectively.

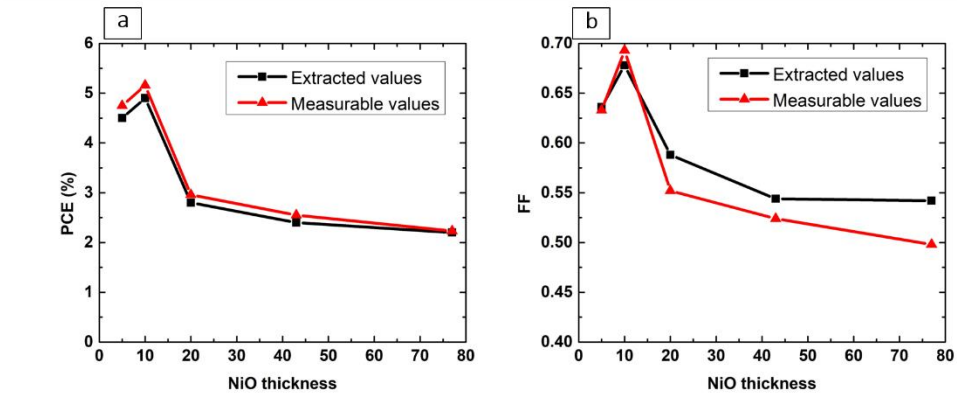

Figure 8: The comparison between extracted and measurable values of PCE (a) and FF (b)

Table 1: The extracted parameters of organic solar cell with NiO buffer layer

NiO thickness	R_s (Ω)	R_{sh} (Ω)	**FF**	**PCE (%)**	Error (%)	
					FF	PCE
05 nm	1.100	584.948	**0.636**	**4.5**	0.47	5.3
10 nm	1.400	3960.108	**0.678**	**4.9**	2.1	5
20 nm	5.771	588.501	**0.588**	**2.8**	6.5	5.4
43 nm	8.585	486.750	**0.544**	**2.4**	3.8	5.9
77 nm	9.341	554.866	**0.542**	**2.2**	8.8	3

Table 2: The measurable parameters of organic solar cell with NiO buffer layer

NiO thickness	V_{OC} (V)	J_{SC} (mA/cm^2)	**FF**	**PCE (%)**
05 nm	0.634	11.5	**0.633**	**4.75**
10 nm	0.638	11.3	**0.693**	**5.16**
20 nm	0.591	8.83	**0.552**	**2.96**
43 nm	0.586	8.09	**0.524**	**2.55**
77 nm	0.581	7.49	**0.498**	**2.23**

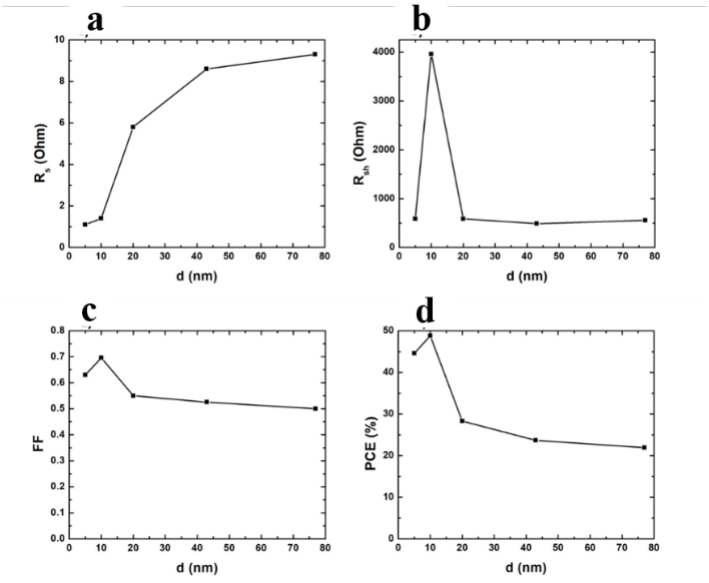

Figure 9: R_s (a), R_{sh} (b), FF (c), and PCE (d) vary in NiO thickness

Fig. 9. provides the change of R_s and R_{sh} under the variation of thickness of NiO. In particular, R_s and R_{sh} influence strongly on the shape of $J-V$ characteristic. If R_s gets smaller and R_{sh} gets larger, the shape of $J-V$ is wider, and vice versa. With the increase of thickness of NiO buffer layer, R_s would increase steadily, whereas R_{sh} would increase until reaching maximum value and then it would decrease dramatically.

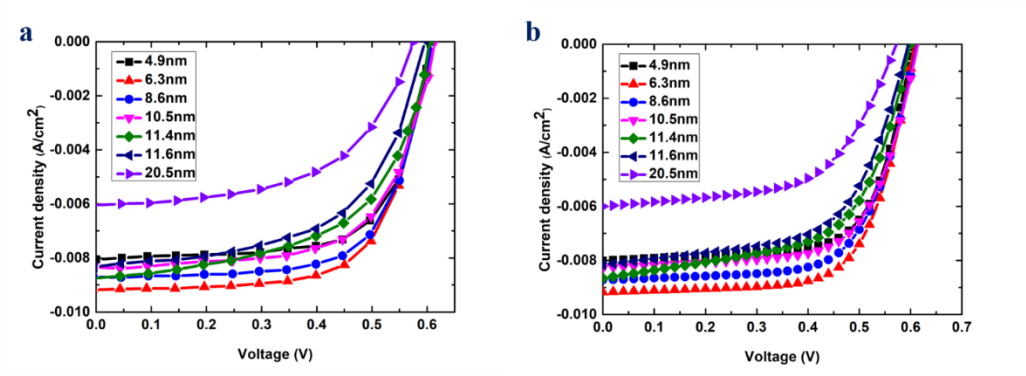

Figure 10: J-V characteristics vary in thickness of ZnO with experimental data (a) and simulated data (b)

Another result based on Chi's data with ZnO cathode buffer layer [1]. Fig. 10 shows the simulated results and measurable data with different thickness of ZnO layer. This indicates that the behavior of simulated data is quite similar to measurable data. From measurable data the extracted parameters are computed and they are represented in the variation of thickness of ZnO as shows in Fig. 10. Remarkably, R_s and R_{sh} values fluctuate in the rage of 5-10 nm of thickness. This fluctuation can stem from as following statement. In the small charge of thickness R_s and R_{sh} depend strongly on the surface roughness of ZnO layers [18]. In contrast, the maximum values of FF and PCE are obtained at 4 nm of ZnO thickness. Therefore, it needs to reduce the surface roughness to gain better PCE.

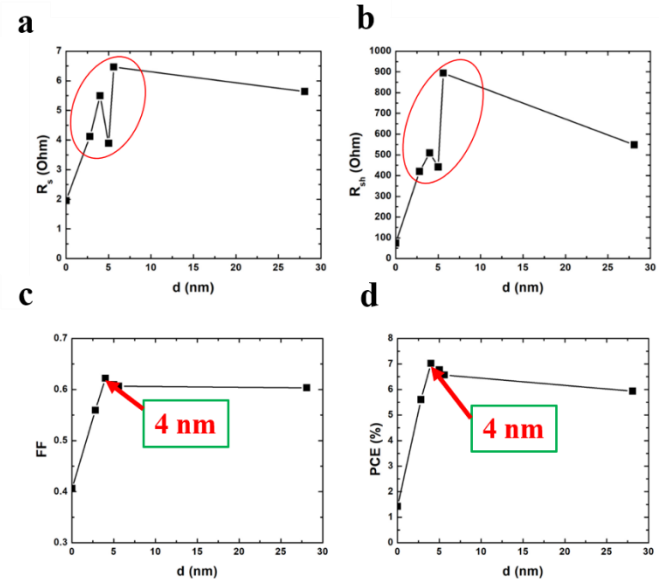

Figure 11: R_s (a), R_{sh} (b), FF (c), and PCE (d) with different ZnO thickness

From the results of dependent on buffer layer thickness, the thickness of buffer layer influences highly on solar cell parameters. For R_s and R_{sh}, these values change sensitively with the thickness of buffer layer, however, this change is quite complicated. In the case of NiO buffer layer, there is steady increase of R_s in the rise of NiO thickness, while R_{sh} reaches a peak of 3960.108 Ω at 10 nm NiO thickness. On the other hand, both R_s and R_{sh} values fluctuate under the small change of ZnO thickness. Overall, despite the different change of both types of resistances, FF and PCE shown the same trend that their values rise steadily, reaching a peak at 4 nm of ZnO thickness and then decreasing with the rise of ZnO thickness. In order to analyze this trend, it is noticed that buffer layers play a role of selective/blocking carriers corresponding with suitable electrodes. With thin buffer layer, it shows the improvement of PCE of organic solar cell compared with the structure which has no buffer layer. This improvement would reach maximum at an optimal layer thickness and then decline sharply. When buffer layer thickness gets the values, which is over the optimal thickness, PCE would decreases because the way for carriers traveling to electrodes is too long. This reduction is as a result of a great proportion of charge carriers lose due to the combination and trapping processes.

Based on the discussion above, it shown that the mechanism of charge carrier lose is analyzed in the macro level, so that the equivalent model cannot reflect intensively the mechanism of charge carrier lose. Therefore, the hopping

transport model is applied with the assistance of Monte Carlo technique for charge transport study in disordered materials as well as organic materials which is component of active layer.

III.2 Charge transport in organic materials

As mention above, the hopping transport model is applied in this work and the input of this model is energy distribution and site distribution in space of film. Here the energy distribution follows Gaussian distribution and the sites are placed in square lattice (in the case of 2D).

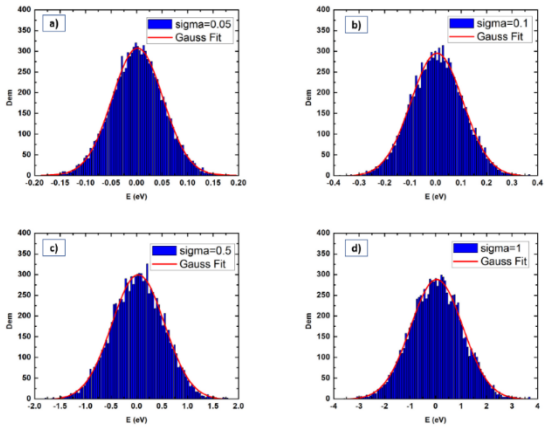

Figure 12: Gaussian distributions with different standard deviations

Making sure that the generated energy distributions are Gaussian, a program was written independently to examine these data. Fig. 12 shows that the generated energy distributions fit well with the Gaussian distribution with mean weigh of 0 and the various standard deviations (sigma). Fig. 13 illustrates the energy landscapes of three different types of distributions including uniform, exponential, and Gaussian distributions over the space.

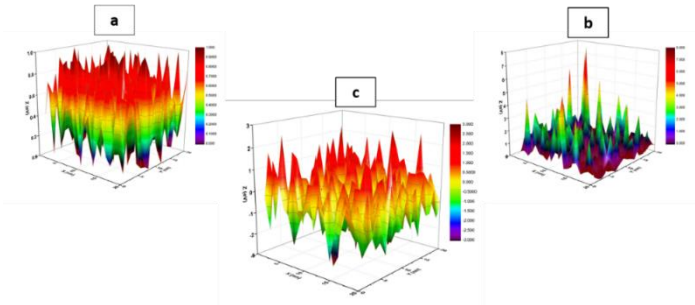

Figure 13: Energy landscapes of three different distributions: uniform distribution (a); exponential distribution (b); Gaussian distribution (c).

Fig. 14 shows the trajectories of single charge carrier that move in lattice. It can be clearly seen that the displacements of carrier spread over the range of electric filed applied in x direction. More detail, Fig. 15 indicates that the mobility of charge carrier increases with rising temperature and electric field, in agreement with theorical prediction.

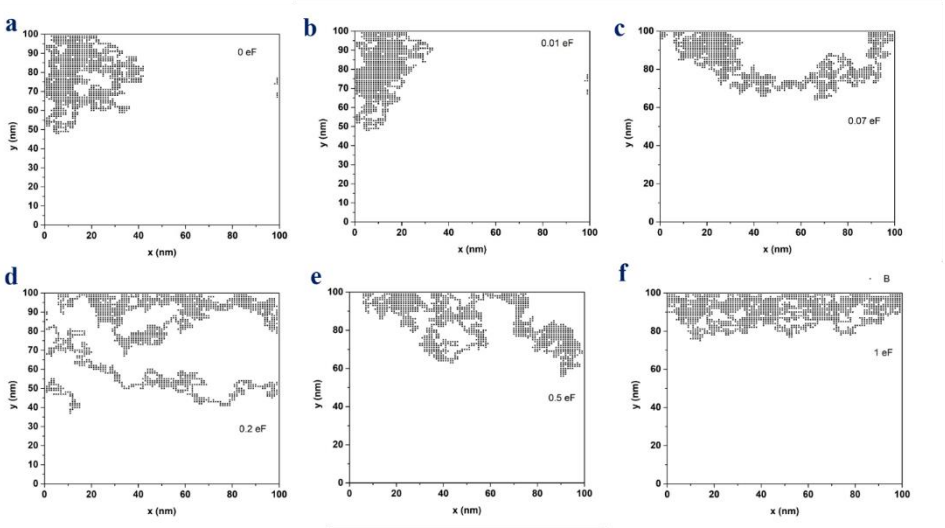

Figure 14:The trajectories of charge carriers under different applied fields

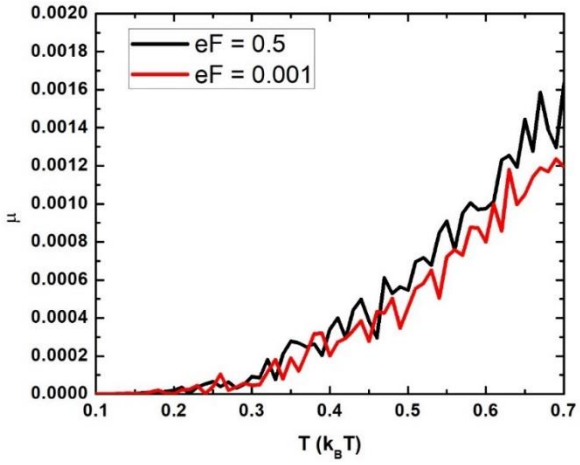

Figure 15: The mobility of charge carrier changes under the variations of temperature and electric field.

VI. Conclusions

To sum up, the single diode model is totally suitable for simulating working principle of organic solar cells and extracting parameters with high accuracy. Based on single diode model, the buffer layer influence solar cell parameters had been shown that the existence of an optimal buffer layer thickness to attain maximum PCE. Besides, the performance of solar cell not only depends on buffer layer thickness but also on the roughness of buffer surface. From our calculation, it shown that when the buffer layer thickness increases, the series resistance would increase, however, the shunt resistance would reach highest value and decrease sharply without roughness factor. A model to simulate the conductivity of organic materials basing on Monte Carlo method has been given and successfully described the charge transport mechanism in a specific material system.

References

[1] D. Chi, S. Huang, S. Yue, K. Liu, S. Lu, Z. Wang*, et al.*, "Ultra-thin ZnO film as an electron transport layer for realizing the high efficiency of organic solar cells," *RSC Advances,* vol. 7, pp. 14694-14700, 2017.

[2] S. D. Baranovskii, "Theoretical description of charge transport in disordered organic semiconductors," *physica status solidi (b),* vol. 251, pp. 487-525, 2014.

[3] K. A. Mazzio and C. K. Luscombe, "The future of organic photovoltaics," *Chemical Society Reviews,* vol. 44, pp. 78-90, 2015.

[4] Z. He, C. Zhong, S. Su, M. Xu, H. Wu, and Y. Cao, "Enhanced power-conversion efficiency in polymer solar cells using an inverted device structure," *Nat Photon,* vol. 6, pp. 591-595, 09//print 2012.

[5] C. Yan, S. Barlow, Z. Wang, H. Yan, A. K. Y. Jen, S. R. Marder*, et al.*, "Non-fullerene acceptors for organic solar cells," *Nature Reviews Materials,* vol. 3, p. 18003, 02/13/online 2018.

[6] N. Yeh and P. Yeh, "Organic solar cells: Their developments and potentials," *Renewable and Sustainable Energy Reviews,* vol. 21, pp. 421-431, 2013/05/01/ 2013.

[7] R. Po, C. Carbonera, A. Bernardi, and N. Camaioni, "The role of buffer layers in polymer solar cells," *Energy & Environmental Science,* vol. 4, pp. 285-310, 2011.

[8] S. Han, W. S. Shin, M. Seo, D. Gupta, S.-J. Moon, and S. Yoo, "Improving performance of organic solar cells using amorphous tungsten oxides as an interfacial buffer layer on transparent anodes," *Organic Electronics,* vol. 10, pp. 791-797, 2009/08/01/ 2009.

[9] C. Tao, S. Ruan, X. Zhang, G. Xie, L. Shen, X. Kong*, et al.*, "Performance improvement of inverted polymer solar cells with different top electrodes by introducing a MoO3 buffer layer," *Applied Physics Letters,* vol. 93, p. 193307, 2008.

[10] M. Yoosuf Ameen, S. Pradhan, M. Remyth Suresh, and V. S. Reddy, "MoO3 anode buffer layer for efficient and stable small molecular organic solar cells," *Optical Materials,* vol. 39, pp. 134-139, 2015/01/01/ 2015.

[11] M. Y. Ameen, P. Shamjid, T. Abhijith, and V. S. Reddy, "Solution processed transition metal oxide anode buffer layers for efficiency and stability enhancement of polymer solar cells," *Optical Materials,* vol. 75, pp. 491-500, 2018/01/01/ 2018.

[12] H. Bässler, "Charge Transport in Disordered Organic Photoconductors a Monte Carlo Simulation Study," *physica status solidi (b),* vol. 175, pp. 15-56, 1993.

[13] A. M. Humada, M. Hojabri, S. Mekhilef, and H. M. Hamada, "Solar cell parameters extraction based on single and double-diode models: A review," *Renewable and Sustainable Energy Reviews,* vol. 56, pp. 494-509, 2016/04/01/ 2016.

[14] K. Ishaque, Z. Salam, and H. Taheri, "Simple, fast and accurate two-diode model for photovoltaic modules," *Solar Energy Materials and Solar Cells,* vol. 95, pp. 586-594, 2011/02/01/ 2011.

[15] D. P. Kroese, T. Brereton, T. Taimre, and Z. I. Botev, "Why the Monte Carlo method is so important today," *Wiley Interdisciplinary Reviews: Computational Statistics,* vol. 6, pp. 386-392, 2014.

[16] A. Ortiz-Conde, F. J. García Sánchez, and J. Muci, "New method to extract the model parameters of solar cells from the explicit analytic solutions of their illuminated I–V characteristics," *Solar Energy Materials and Solar Cells,* vol. 90, pp. 352-361, 2006/02/15/ 2006.

[17] M. D. Irwin, D. B. Buchholz, A. W. Hains, R. P. H. Chang, and T. J. Marks, "p-Type semiconducting nickel oxide as an efficiency-enhancing anode interfacial layer in polymer bulk-heterojunction solar cells," *Proceedings of the National Academy of Sciences of the United States of America,* vol. 105, pp. 2783-2787, 02/1909/12/received 2008.

[18] H.-Y. Park, D. Lim, K.-D. Kim, and S.-Y. Jang, "Performance optimization of low-temperature-annealed solution-processable ZnO buffer layers for inverted polymer solar cells," *Journal of Materials Chemistry A,* vol. 1, pp. 6327-6334, 2013.